JOURNAL OF GEOPHYSICAL RESEARCH, VOL. 111, B09313, doi:10.1029/2005JB004202, 2006

Detection of ruptures of Andaman fault segments in the 2004 great Sumatra earthquake with coseismic ionospheric disturbances

Kosuke Heki,[1] Yuichi Otsuka,[2] Nithiwatthn Choosakul,[3] Narong Hemmakorn,[4] Tharadol Komolmis,[5] and Takashi Maruyama[6]

Received 2 December 2005; revised 9 March 2006; accepted 16 June 2006; published 23 September 2006.

[1] Near-field coseismic perturbations of ionospheric total electron content (TEC), caused by direct acoustic waves from focal regions, can be observed with Global Positioning System (GPS). They appear 10–15 min after the earthquake with typical periods of ~4–5 min and propagate as fast as ~1 km/s toward directions allowed by ambient geomagnetic fields. Ionospheric disturbance, associated with the 2004 December 26 great Sumatra-Andaman earthquake, was recorded with nine continuous GPS receiving stations in Indonesia and Thailand. Here we explore the possibility to constrain the rupture process of the earthquake with the observed ionospheric disturbances. We assumed linearly distributed point sources along the zone of coseismic uplift extending ~1300 km from Sumatra to the Andaman Islands that excited acoustic waves sequentially as the rupture propagate northward by 2.5 km/s. TEC variations for several satellite-receiver pairs were synthesized by simulating the propagation of acoustic waves from the ground to the ionosphere and by integrating the TEC perturbations at intersections of line of sights and the ray paths. The TEC perturbations from individual point sources were combined using realistic ratios, and the total disturbances were compared with the observed signals. Prescribed ratios based on geodetically inferred coseismic uplifts reproduced the observed signals fairly well. Similar calculation using a rupture propagation speed of 1.7 km/s degraded the fit. Suppression of acoustic waves from the segments north of the Nicobar Islands also resulted in a poor fit, which suggests that ruptures in the northern half of the fault were slow enough to be overlooked in short-period seismograms but fast enough to excite atmospheric acoustic waves. Coseismic ionospheric disturbance could serve as a new indicator of faulting sensitive to ruptures with timescale up to 4–5 min.

Citation: Heki, K., Y. Otsuka, N. Choosakul, N. Hemmakorn, T. Komolmis, and T. Maruyama (2006), Detection of ruptures of Andaman fault segments in the 2004 great Sumatra earthquake with coseismic ionospheric disturbances, *J. Geophys. Res.*, *111*, B09313, doi:10.1029/2005JB004202.

1. Introduction

[2] The great Sumatra-Andaman earthquake ruptured the segment of the plate boundary fault as long as ~1300 km extending from the northwestern coast of Sumatra, Indonesia, to the Andaman Islands on 26 December 2004 (Figure 1). Its moment magnitude (M_w) was initially reported in Harvard centroid moment tensor solution as 9.0 from records of seismic waves radiated mainly from the southern half of the fault [*Lay et al.*, 2005]. Later the magnitude was revised upward as other kinds of observations revealed additional moment slowly released in the northern half extending from the Nicobar to the Andaman Islands. From observations of the Earth's free oscillation, sensitive to slower faulting, *Stein and Okal* [2005] inferred the M_w as 9.3. Using static coseismic displacements obtained by Global Positioning System (GPS), *Banerjee et al.* [2005] estimated fault parameters (Figure 1b) and suggested M_w as 9.2.

[3] It is still controversial how slow the rupture was in the northern half. Tsunami can be excited by slower slips than seismic waves, with timescales up to a few tens of minutes. The tsunami of this earthquake has been recorded by two different sensors; in addition to conventional tide gauges, radar altimeter recorded tsunami height profiles along satellite trajectories [*Lay et al.*, 2005]. They present some

[1]Division of Earth and Planetary Sciences, Hokkaido University, Sapporo, Japan.
[2]Solar Terrestrial Environment Laboratory, Nagoya University, Honohara, Toyokawa-city, Japan.
[3]Department of Geology, Faculty of Science, Chulalongkorn University, Bangkok, Thailand.
[4]Department of Telecommunications, Faculty of Engineering, King Mongkut's Institute of Technology, Bangkok, Thailand.
[5]Department of Electrical Engineering, Faculty of Engineering, Chiang Mai University, Chiang Mai, Thailand.
[6]National Institute of Information and Communications Technology, Tokyo, Japan.

0148-0227/06/2005JB004202$09.00

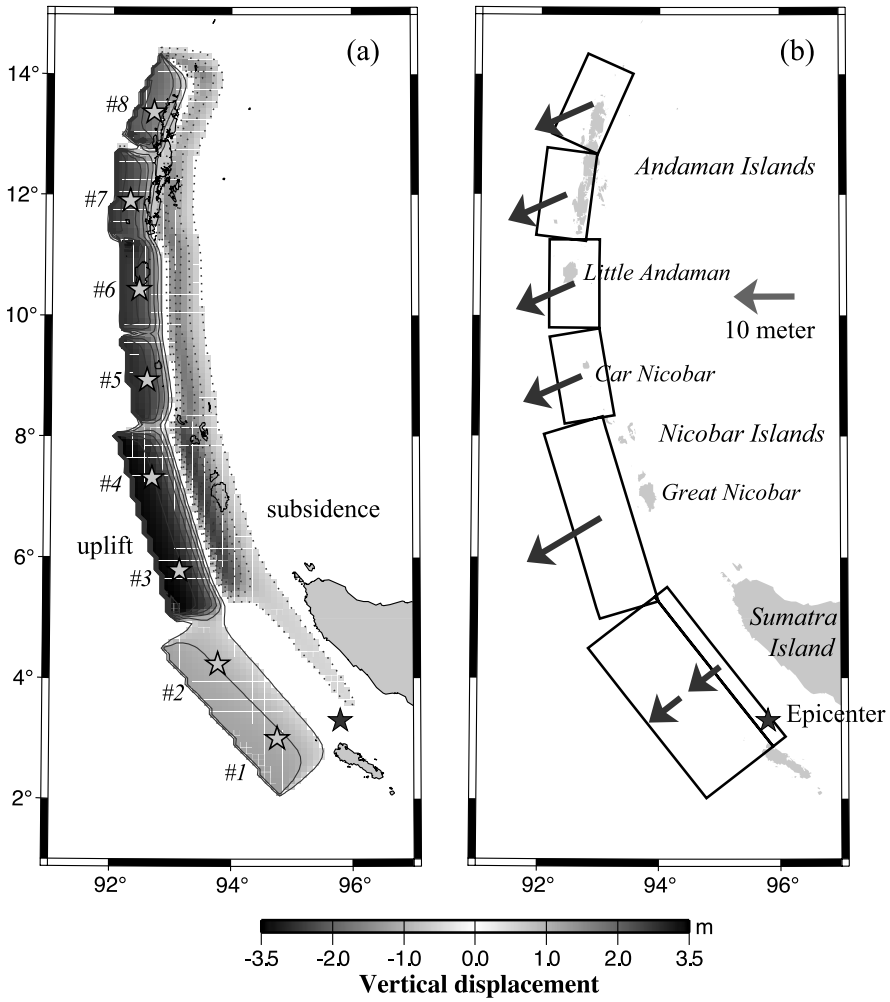

Figure 1. (a) Vertical crustal movements associated with the 2004 Sumatra-Andaman earthquake calculated assuming an elastic half-space [*Okada*, 1992] and fault parameters, model 3 of *Banerjee et al.* [2005]. The contour interval is 50 cm. Gray stars numbered from 1 to 8 denote centers of uplift for the fault divided into eight segments. (b) Fault geometry and coseismic slip vectors. Uplift is much larger in amplitude and area than subsidence.

inconsistency at the moment [e.g., *Fujii and Satake*, 2005]; the former favors tsunamigenic rupture only in the southern half (i.e., slips in the northern half were too slow to excite tsunami) while the latter suggests the tsunami genesis from the entire fault. Recent reanalysis of Indian tide gauge data suggested that the tsunami source extended as north as the Andaman Islands [*Neetu et al.*, 2005].

[4] Microwave suffers from propagation delay inversely proportional to the square of frequency when it penetrates the ionosphere. GPS receivers for precise positioning purposes are designed to receive carrier phases of two different frequencies to remove such ionospheric delays. We can also isolate ionospheric delays by differencing the arrival times of the signals on the two carriers. They are proportional to total electron content (TEC) along the line of sight and provide useful information on ionospheric disturbances. Coseismic ionospheric disturbances (CID) were found to occur following earthquakes in 1960s by Doppler sounding technique [*Yuen et al.*, 1969]. Recent increase of continuous GPS stations enhanced the chance to detect CIDs in terms of TEC variations [*Calais and Minster*, 1995; *Heki and Ping*, 2005].

[5] Such TEC variations are caused by electron density irregularities that occur when atmospheric waves go through the ionosphere. Atmospheric waves include (1) direct acoustic wave from the focal area, (2) gravity wave propagating obliquely upward from the focal area or from propagating tsunami, and (3) secondary acoustic wave excited in areas away from the epicenter by the Rayleigh surface wave (Figure 2). CIDs caused by these three types of waves have been detected by dense GPS arrays after the 2003 Tokachi-oki, Japan [*Heki and Ping*, 2005], the 2001 Peru [*Artru et al.*, 2005], and the 2002 Denali [*Ducic et al.*, 2003] earthquakes, respectively. Similar ionospheric disturbances were found after the 2004 eruption of the Asama Volcano, Central Japan [*Heki*, 2006], which is similar to the first one, i.e., caused by acoustic wave excited by the explosion.

[6] The CID of the third kind propagates as fast as the Rayleigh surface wave (>3 km/s). It is easily separable from

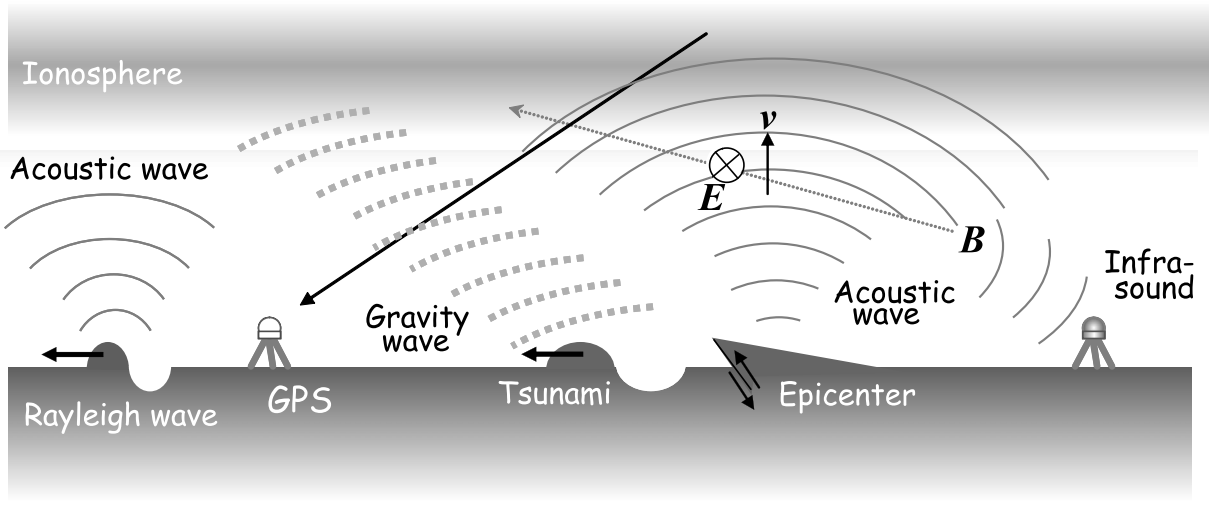

Figure 2. Three kinds of atmospheric waves that disturb ionosphere and can be observed with GPS as TEC changes, i.e., (1) direct acoustic wave from the focal area, (2) gravity wave propagating obliquely upward from the focal area or from propagating tsunami, and (3) secondary acoustic wave excited in far fields by the Rayleigh surface wave. Part of the direct acoustic wave comes back to the ground by atmospheric refraction and is observed by infrasound sensors [*Le Pichon et al.*, 2005]. Vertical movements of ionized particles in the geomagnetic field induce current in ionospheric and cause geomagnetic pulsation [*Iyemori et al.*, 2005].

the first kind (direct acoustic waves from the focal area) that propagates as fast as the sound wave at height (∼1 km/s). *Ducic et al.* [2003] and *Artru et al.* [2004] suggested that the CIDs of the third kind provide useful information on surface wave velocities in oceanic regions where seismometers are not available. Here we study CIDs of the first kind associated with the 2004 December great Sumatra earthquake, and examine the possibility to extract information on the rupture process of large earthquakes through a new time window. CIDs of the third kind were also detected for this earthquake by the dense GPS array in Japan, but they will be reported in a separate article (K. Heki, manuscript in preparation, 2006).

2. Observed Coseismic Ionospheric Disturbances

2.1. GPS-TEC Measurements in Indonesia and Thailand

[7] We used data from two continuous GPS receiving stations in Sumatra, Indonesia; SAMP near Medan, northern Sumatra (Figure 3), and PDNG in Padang, middle Sumatra. We compare TEC time series of SAMP over the same time interval of five consecutive days in Figure 4. Seven stations in Thailand, (from south to north) Phuket (PHKT), Chunpon (CPN), Bangkok (BNKK and KMI), Sri Samrong (SIS2), and Chiang Mai (CHMI and CMU), also showed significant CIDs (Figure 5). The TEC time series from the two stations in Bangkok and Chiang Mai were almost identical reflecting their spatial proximity. Data of nearby IGS (International GPS Service) stations in Singapore, Java, Cocos Island, did not show clear CID. Sampling intervals are 10 s at CPN, and 30 s at other points. A recent report by *DasGupta et al.* [2006] suggests that disturbance expanded as far as Kolkata, eastern India. A part of the data presented here has been reported already by *Otsuka et al.* [2006] without substantial discussions on the earthquake source processes.

[8] Our GPS data analysis procedure follows earlier studies [*Calais and Minster*, 1995; *Calais et al.*, 1998]: (1) the L1 (∼1.5 GHz) and L2 (∼1.2 GHz) carrier phases in original data files were converted to lengths by multiplying with the wavelengths and (2) their differences (ionospheric linear combinations) were multiplied with a factor into TEC. Biases in TEC coming from integer ambiguities of the phases were not removed because they are constant and irrelevant to CID, short-term TEC changes. Such data are geometry-free, i.e., sensitive only to ionospheric delay changes but insensitive to receiver displacements and neutral atmospheric delays.

[9] The TEC time series over the 1.1 hour interval (from 0054 to 0200 UT) have been low-cut filtered by subtracting degree three polynomials fit to them. Figure 3 shows TEC time series from eight satellites received at SAMP. In Figure 3 are also shown trajectories of subionospheric point (SIP), ground projections of intersections between the line of sights and the ionosphere modeled as a thin shell as high as 300 km. Three satellites (13, 20, and 23), with SIPs relatively close to the epicenter, showed significant CIDs. They were of the order of a few TEC units (1 TECU = 10^{16} el/m^2), an order of magnitude larger than those of the 2003 Tokachi-oki earthquake (M_w 8.0), Japan [*Heki and Ping*, 2005]. Such disturbances are seen only on 26 December (Figure 4), suggesting that they are caused by the earthquake rather than diurnally repeating solar-terrestrial phenomena such as the traveling ionospheric disturbance (TID) by moving solar terminator [*Galushko et al.*, 1998].

[10] In Figure 5, we compare SIP trajectories and TEC time series of satellites 13, 20, and 23 observed at the nine (eight) GPS stations (PDNG did not show significant CIDs for satellites 20 and 23). *Heki and Ping* [2005] obtained the apparent velocity of ∼1 km/s for the 2003 Tokachi-oki earthquake, by drawing the travel time diagram taking the along-surface distances between the SIPs and the center of

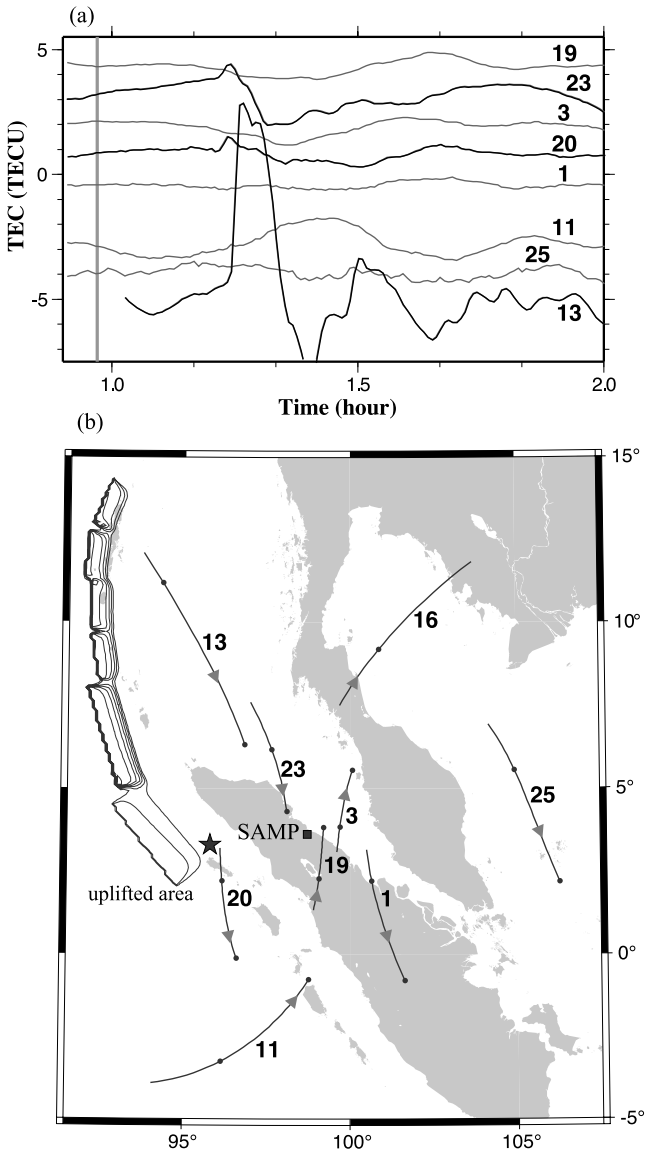

Figure 3. (a) TEC time series 0054 to 0200 UT observed at SAMP with eight satellites. The vertical line shows the rupture start time (00:58:53 UT). Ionospheric disturbances are seen for Sat.13, Sat.20, and Sat.23 (bold curves). (b) SIP trajectories over the same period. Solid circles on the trajectories denote time marks for 0100 UT and 0200 UT. Uplift contours are same as Figure 1a. GPS satellite numbers are shown in Figures 3a and 3b.

the uplifted area as the focal distances. In the present case, coseismic uplift region elongates along the fault, and the focal distance cannot be simply defined. We take the time lag of disturbance peak arrivals for satellite 13 (Figure 5a) between BNKK and CPN, both of which are relatively distant from the source. Their focal distances are different by ~400 km. The time lag of the peak arrivals is ~7 min, suggesting the approximate propagation speed of ~1 km/s. This roughly coincides with the sound velocity at ionospheric height, and indicates that these were the CID of the first kind, i.e., caused by the direct acoustic wave from the focal region.

[11] *Kanamori et al.* [1994] and *Tahira* [1994] suggested that the resonance between the solid earth and atmospheric sound wave occurs at a period of ~4.5 min (~3.7 mHz), and this coincided with the typical CID period found in the 2003 Tokachi earthquake [*Heki and Ping*, 2005]. This period also serves as the cutoff; that is, ground movements of longer periods do not excite sound wave (they instead generate gravity waves). In Figure 5, apparent CID periods are similar to this resonance period at SIPs relatively close to the epicenter (e.g., PHKT-Sat.20 and PDNG-Sat.13), but tend to get longer as they propagate farther exceeding the acoustic cutoff period (e.g., CMU-Sat.13, 20, 23). This might be an apparent phenomenon caused by the combina-

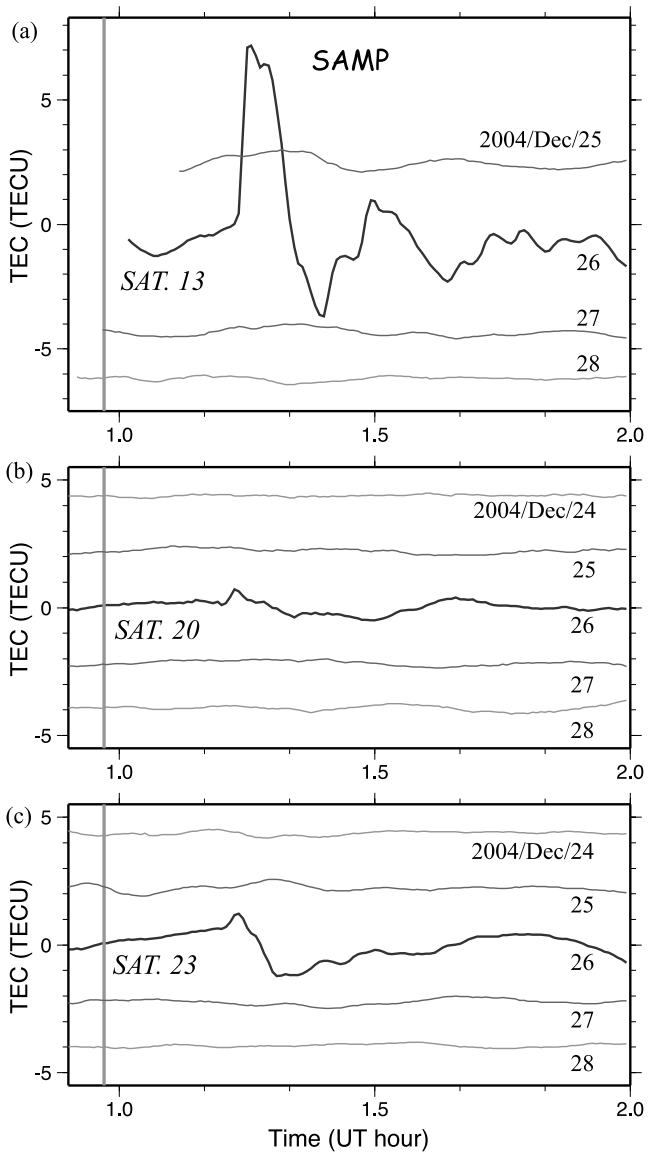

Figure 4. TEC time series 0054 to 0200 UT observed at SAMP with the satellite (a) 13, (b) 20, and (c) 23, on the five consecutive days (24–28 December 2004). The vertical line shows the rupture start time on 26 December (0058:53 UT). Ionospheric disturbances are seen only on 26 December, the day of the earthquake. Satellite 13 was not observed on the first day (24 December).

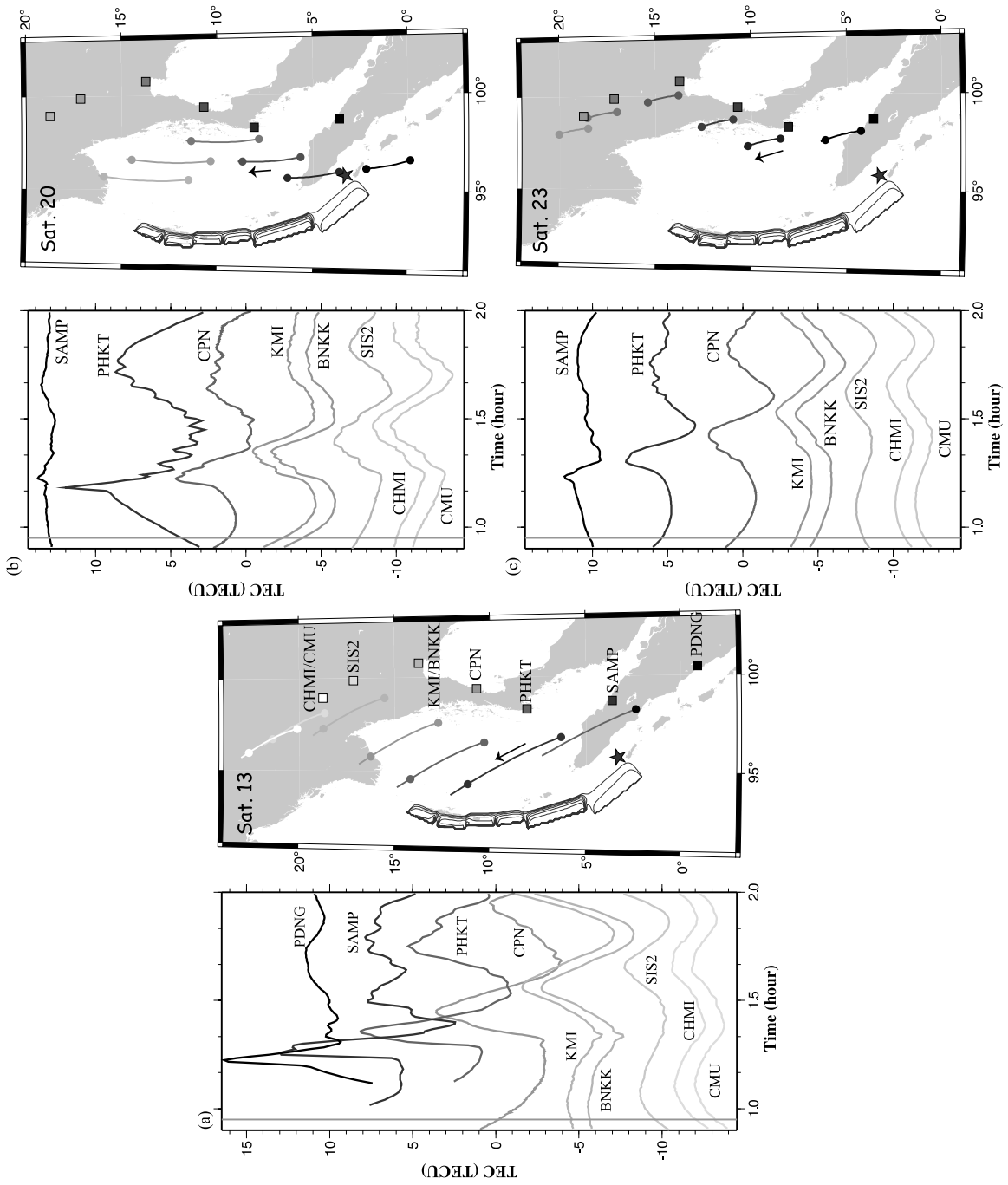

Figure 5. TEC time series and the SIP trajectories 0054 to 0200 UT of the GPS (a) Sat.13, (b) Sat.20, and (c) Sat.23. The names and locations of GPS stations are shown in Figure 5a. KMI/BNKK (Bangkok, Thailand) and CHMI/CMU (Chiang Mai, Thailand) stations are only ~20 km and ~4 km apart from each other. Ionospheric disturbances appear ~10 min after the earthquake at the nearest SIP and start to propagate. Arrows indicate moving directions of the SIP.

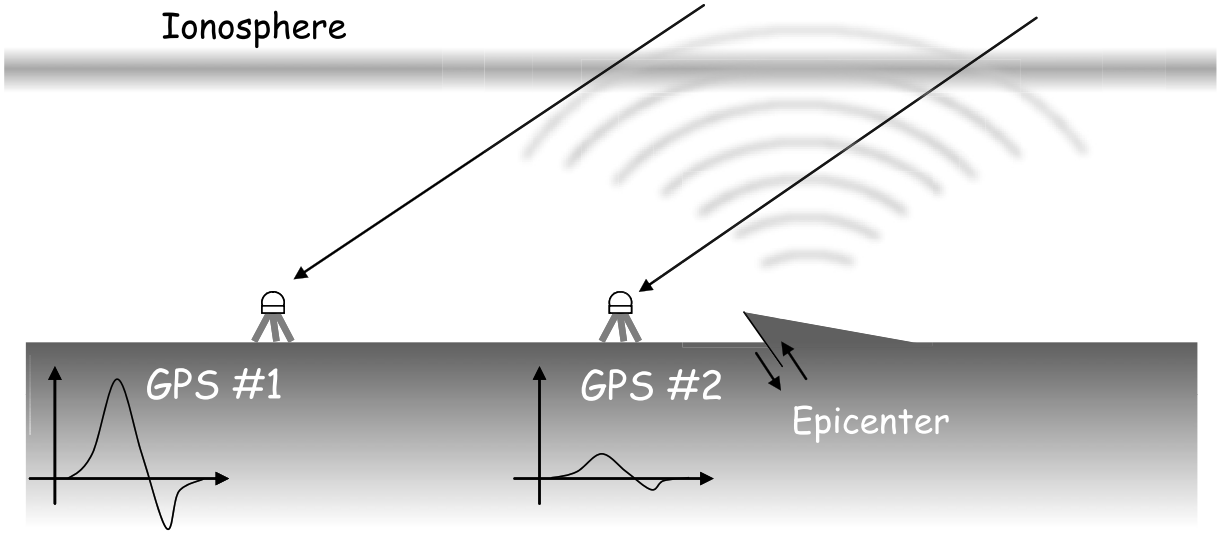

Figure 6. Amplitude of the observed disturbance depends on the angle between the wave front and the line of sight, i.e., the amplitude gets larger if they are parallel at the ionospheric height (GPS 1).

tion of sequentially arriving CIDs with a shorter period excited at various points in the uplifted region. This may also reflect dispersion of acoustic waves of unknown origin that blurs wave front gradually.

2.2. Comparison With Relevant Observations

[12] Solar flares promote ionization and cause sudden increase in TEC with timescales similar to CID [e.g., *Zhang and Xiao*, 2005]. We confirmed that no solar flares are reported on 26 December 2004 in the Web page of the Space Environment Center (http://www.sec.noaa.gov). Solar flares cause simultaneous TEC increases for the whole sunlit hemisphere, and look different from CID having finite propagation speed. Also we can rule out large- and medium-scale TIDs irrelevant to the earthquake because they are internal gravity waves with apparent velocities of a few hundreds of meters per second [*Saito et al.*, 2002].

[13] Here we examine several other kinds of geophysical observations of the 2004 Sumatra earthquake that may have some relationship with the observed CID. *Le Pichon et al.* [2005] reported detection of infrasound signals by array sensors at Diego Garcia, Indian Ocean. They are considered to be acoustic waves that have been launched with lower angles from the epicenter and have been refracted back to the surface without reaching ionosphere (Figure 2). They have more complicated signatures being dominated by shorter-period waves than the observed CID. The loss of short-period components in the CID might be due to the atmospheric filter, i.e., acoustic waves with periods shorter than 0.5–1.0 min are strongly attenuated by atmosphere at elevations >100 km [*Georges*, 1968].

[14] *Liu et al.* [2006] reported ionospheric disturbances by the 2004 Sumatra earthquake observed with the Doppler sounder array in Taiwan. The disturbance passed through the array twice; the first one ~20 min and the second one >3 hours after the earthquake. They are considered to be the secondary acoustic wave excited by the passage of the Rayleigh wave (speed ~3.6 km/s), and atmospheric gravity wave (speed ~360 m/s), respectively (Figure 2). Direct acoustic waves from the epicenter would have decayed before reaching Taiwan. *Iyemori et al.* [2005] reported geomagnetic pulsation ~13 min after the earthquake in Thailand. They attributed it to the electric current in the ionospheric E layer induced by the Lorentz force exerted on the vertically oscillating charged particles in the acoustic wavefront (Figure 2). This pulsation is a phenomenon directly related to the CID observed in the present study.

3. Synthesized Disturbances

3.1. Waveform and Relative Amplitudes

[15] Uplift associated with a thrust earthquake makes a dense atmospheric mass above the ground, which starts to propagate upward as acoustic wave. Sound velocity scales with the square root of the temperature. The temperature gradually decreases as the wave goes up, and becomes minimal at the mesopause as high as ~90 km, and then increases asymptotically toward a plateau at ~1000 K above the height ~300 km. The increasing velocity with altitude refracts the ascending waves downward.

[16] Following *Calais et al.* [1998], *Heki and Ping* [2005] performed a simple ray tracing in the atmosphere under such velocity structure, and predicted the TEC change at various epochs by integrating the instantaneous ΔTEC values at the intersections of individual ray paths with the satellite to receiver line of sight. *Heki and Ping* [2005] assumed a bipolar source function composed of a positive part (i.e., dense atmospheric mass above the uplifted crust) and a smaller follow-on negative part, and let it propagate along ray paths with launching angles taken every 0.5 degree. The amplitude of the source function was adjusted a posteriori to make the predicted CID coincide with the observed signals. This method successfully reproduced the waveforms, arrival times, and relative amplitudes of the observed CID.

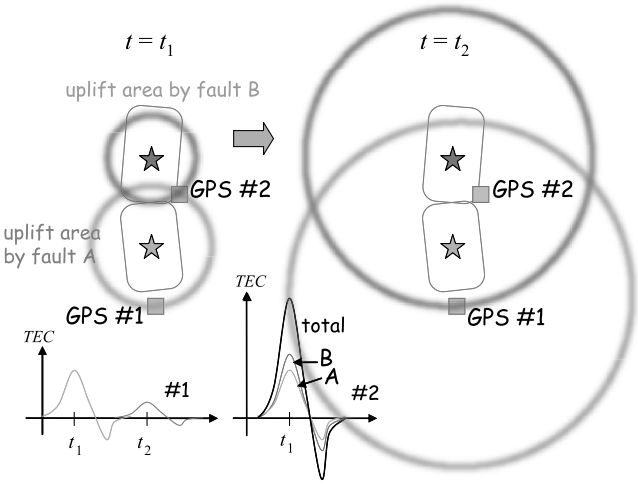

Figure 7. Combination of CID due to two point sources where acoustic waves are excited successively (faults A and B). The CID wave fronts from the two arrive at the SIP of GPS 2 simultaneously, and the signals are enhanced. At the SIP of GPS 1, the CIDs arrive separately.

[17] Three major factors influence the waveforms and amplitudes of CID: (1) distance from the source, (2) incidence angle of the line of sight (Figure 6), and (3) directivity caused by geomagnetism. If CID signals from different point sources overlap, their phase difference becomes a major factor, too (Figure 7). TEC disturbance decays as the wave travels away from the source due to the first factor, but observed CID amplitude is not a simple function of focal distance due to the second factor. The source function is made of positive and negative parts, and they partly cancel each other when the line of sight is not parallel with the wave front. So a GPS station nearer to the epicenter could record a smaller CID than the other station farther from the source (Figure 6).

[18] The directivity of CID (the third factor) occurs because electrons can move only along the ambient geomagnetic field [*Hooke*, 1970]; that is, only acoustic wave with front perpendicular to the field survives in the ionosphere. This directivity is latitude-dependent, e.g., southward in the midlatitude of the Northern Hemisphere. In equatorial region like Sumatra, two beams extend northward and southward, that is, acoustic waves propagating eastward or westward are diminished in the ionosphere by the northward/horizontal geomagnetic field. Such directivity is taken into account in synthesizing CID signals following *Heki and Ping* [2005], but its role is relatively minor here because the sources are dispersed along a finite length (an SIP, located due east of one source, is not due east of the others).

3.2. Excitation Sources

[19] We repeat the same method to synthesize CID variation for a point source as *Heki and Ping* [2005], for the eight point sources located in a row (Figure 1a), and let the synthesized CIDs interfere with one another. Here we assume the parameters of the fault segments by *Banerjee et al.* [2005], estimated to fit coseismic displacements of GPS stations. They are all low-angle shallow thrust faults except the southernmost segment where an additional segment was assumed at its downdip extension (Figure 1b).

[20] These fault parameters predict coseismic vertical displacements in the near field shown in Figure 1a. Here we assume eight point sources of CID that correspond to along-strike fault segments. The two southernmost segments (those south of 8N) were split into two to equalize the areas represented by the point sources (the deeper segment of the southernmost one is also split and attached to the shallower part). Relative amplitudes of excited acoustic waves at these sources (Figure 8a) were assumed proportional to the average uplift by the individual segments at grid points showing uplifts >50 cm (the outermost contour line in Figure 1a). The points are located at the centers of the uplifted areas and are numbered from 1 to 8 (Figure 1a). The sources 3 and 4 are the strongest due to the large dislocation and uplift, while the sources 1 and 2 are relatively small because of small dislocation of the shallow fault segment. The strengths of northern sources could be significantly smaller if the fault rupture there had been too slow.

[21] Exact times of the acoustic wave generations at the eight point sources have been calculated assuming the rupture onset at 0058:53 UT at (3.3°N, 96.0°E) and a constant propagation speed of 2.5 km/s [*Ammon et al.*, 2005; *Lay et al.*, 2005]. Tsunami waveform analyses sug-

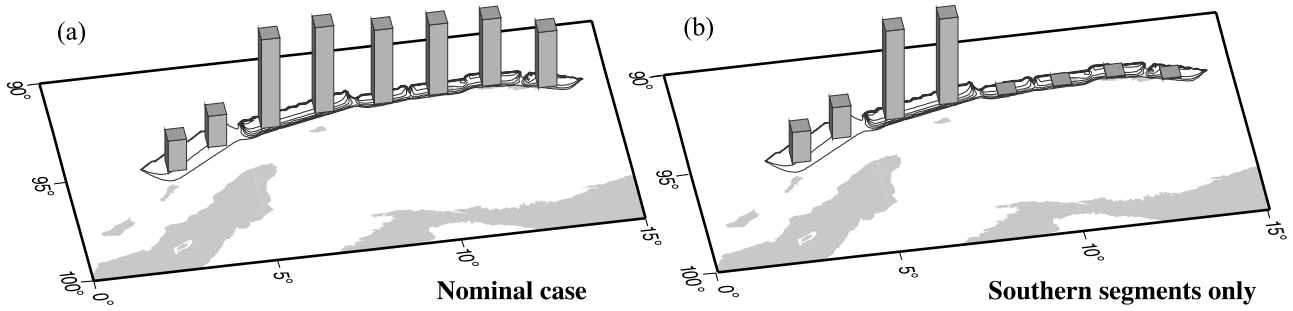

Figure 8. Relative amplitudes of acoustic waves excited at the eight point sources, the centers of uplifted regions by eight fault segments (Figure 1a). (a) Nominal case. They were assumed to be proportional to the average values of uplifts at grid points showing >50 cm uplift. (b) Southern segments only. We also considered an optional model where ruptures in the northern half were too slow to generate acoustic waves.

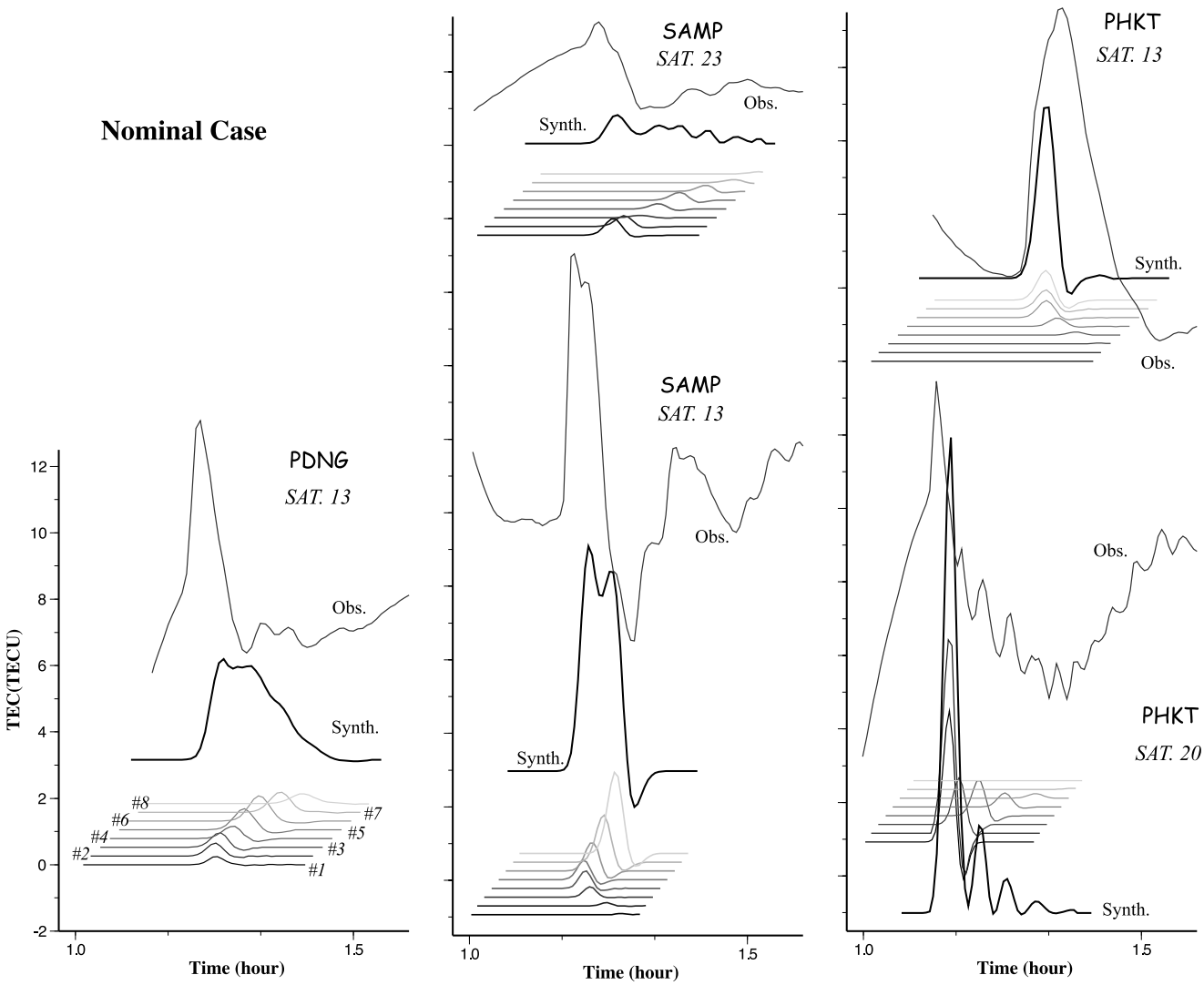

Figure 9. Synthesized CIDs by the eight point sources, shown in Figure 1, shown as eight gray curves (darker curves denote more southerly sources, and with 1–8 corresponding to those in Figure 1a). They were combined by the prescribed ratio (Figure 8a) to compare the total synthesized CID (black) with the observed ones (gray). The stations, (left) PDNG, (middle) SAMP, and (right) PHKT, and satellite numbers (Sat.13, Sat.20, and Sat.23) are shown. The rupture propagation speed is assumed to be 2.5 km/s.

gested that rupture propagation speed as slow as 1.7 km/s resulted in a better fit [e.g., *Tanioka et al.*, 2006]. Later we will compare CIDs synthesized using these two different velocities.

3.3. Synthesis of CID Signals: Nominal Case

[22] In Figure 9 we plot such synthesized CIDs from the eight point sources 1–8. They are based on uniform source magnitudes, but the three factors (distance, incidence angle, and directivity) have already given different amplitudes and arrival times as CIDs for them. Here we combine them with relative weights shown in Figure 8a, and compare resultant CIDs with the observed ones. Figure 9 shows the nominal case where rupture propagation speed of 2.5 km/s is used. In the Figures 9, 10, and 11, only the relative amplitudes, waveforms, and arrival times are meaningful because uniform arbitrary scaling to the synthesized signals has been performed.

[23] The synthesized signals resemble the observed CIDs to some extent. The two pairs SAMP-Sat.23 and SAMP-Sat.13 (Figure 9, middle) represent the two extreme cases of arrivals of CIDs from point sources. Arrivals are discrete for the former and the total signal does not have a strong peak. The phases of the point sources are fairly coherent for the latter, resulting in a high peak of the combined CID. The PHKT-Sat.13 and PHKT-Sat.20 (Figure 9, right) show another kind of two extreme cases in the fault segments the total CIDs reflect; the former is caused mainly by the northern half of the fault (5–8) while the contribution from the southernmost two sources (1–2) are dominant in the latter.

[24] The observed and the synthesized curves differ in several aspects. As for arrival times, the synthesized CIDs are uniformly late in time by a few minutes (except for PHKT-Sat.13). This might reflect either a certain difference between the real and assumed atmospheric sound velocity

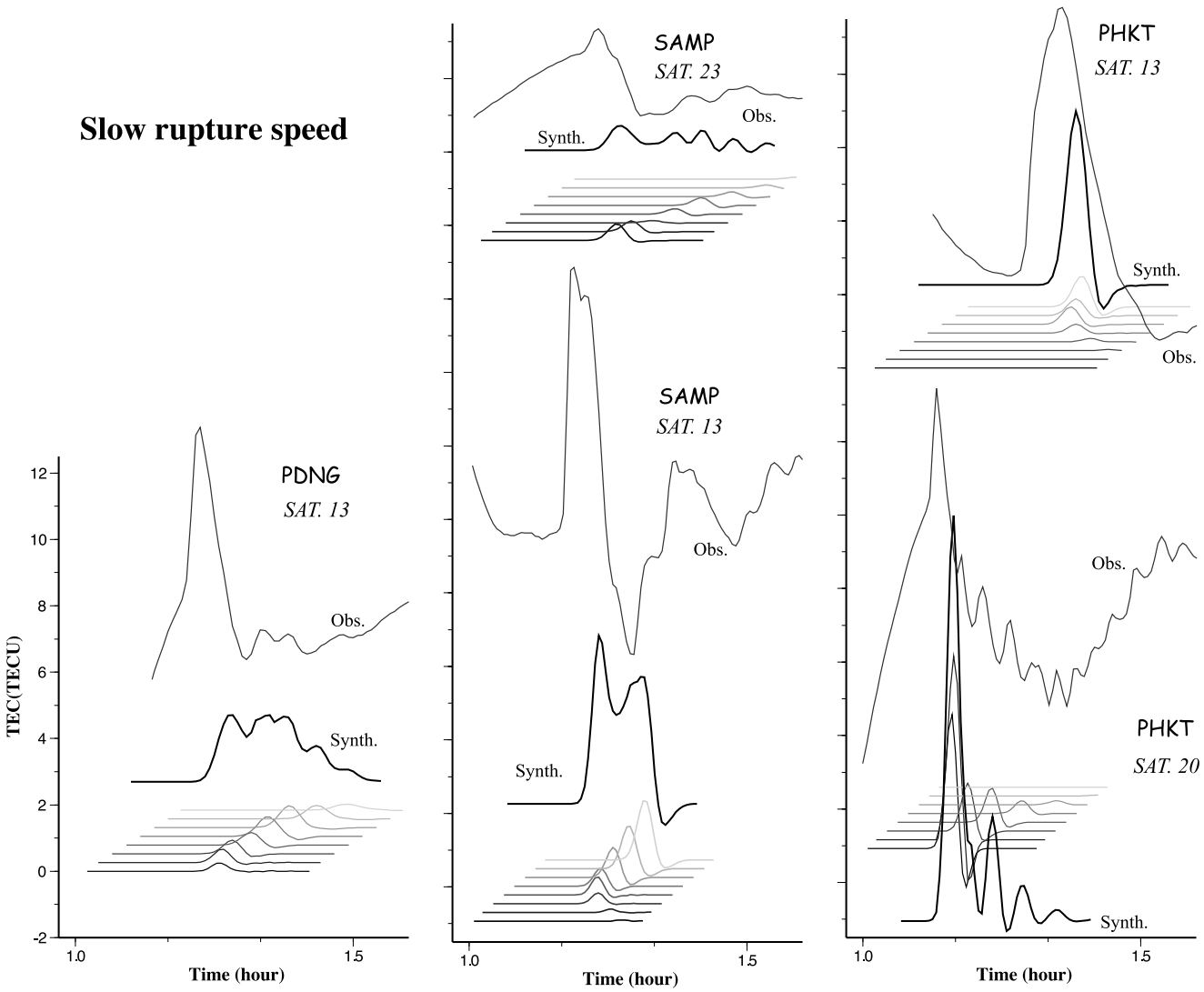

Figure 10. Same as Figure 9, but the rupture propagation speed reduced to 1.7 km/s.

structure, or the slowness of the rupture during the initial ~1 min of the rupture as suggested by *Ammon et al.* [2005]. The synthesized waveform is not very consistent with the observed CID for PDNG-Sat.13 (observed CID has a stronger peak than the synthesized one). Such a low semblance could be improved by "tuning" the relative amplitudes of the sources, e.g., by increasing the strengths of the sources 3 and 4. This will be discussed later.

3.4. Synthesis of CID Signals: Optional Cases

[25] Next we examine two optional cases: (1) to reduce the rupture propagation speed to 1.7 km/s and (2) to suppress the CID excitation in the northern half of the fault. Figure 10 shows the first optional case, where excitations of the acoustic waves at the northerly point sources were delayed due to the slower rupture propagation. The total rupture duration increases from 520 s to 765 s, i.e., the rupture of the northernmost segment lags behind by ~4 min. This makes the phases of CIDs from the eight sources less coherent for SAMP-Sat.13 and PDNG-Sat.13, and their synthesized CIDs lose high peaks as seen in Figure 10. We therefore consider the slow rupture propagation as proposed by *Hirata et al.* [2006] (<1.0 km/s) and *Tanioka et al.* [2006] (~1.7 km/s) less likely, although a nonuniform speed model, e.g., faster/slower propagation for the southern/northern half of the fault, might rather result in an improved fit.

[26] Figure 11 shows the second optional case, where the TEC disturbances from the northern half have been suppressed (Figure 8b). This would have been the case if time constant of the rupture there had been longer than the acoustic cutoff. The large synthesized CIDs, which were seen for SAMP-Sat.13 and PHKT-Sat.13 in Figure 9, disappear in Figure 11. On the other hand, PHKT-Sat.20 and SAMP-Sat.23 are little influenced by the change. Thus the synthesized and observed CIDs of these four pairs cannot be reconciled by simply rescaling the former. After all, the observed CIDs suggest that acoustic waves from the northern fault segments, beneath the Andaman Islands, must exist. The northern half of the fault segments would have undergone movements slow enough to be overlooked by seismometers but fast enough to excite atmospheric acoustic

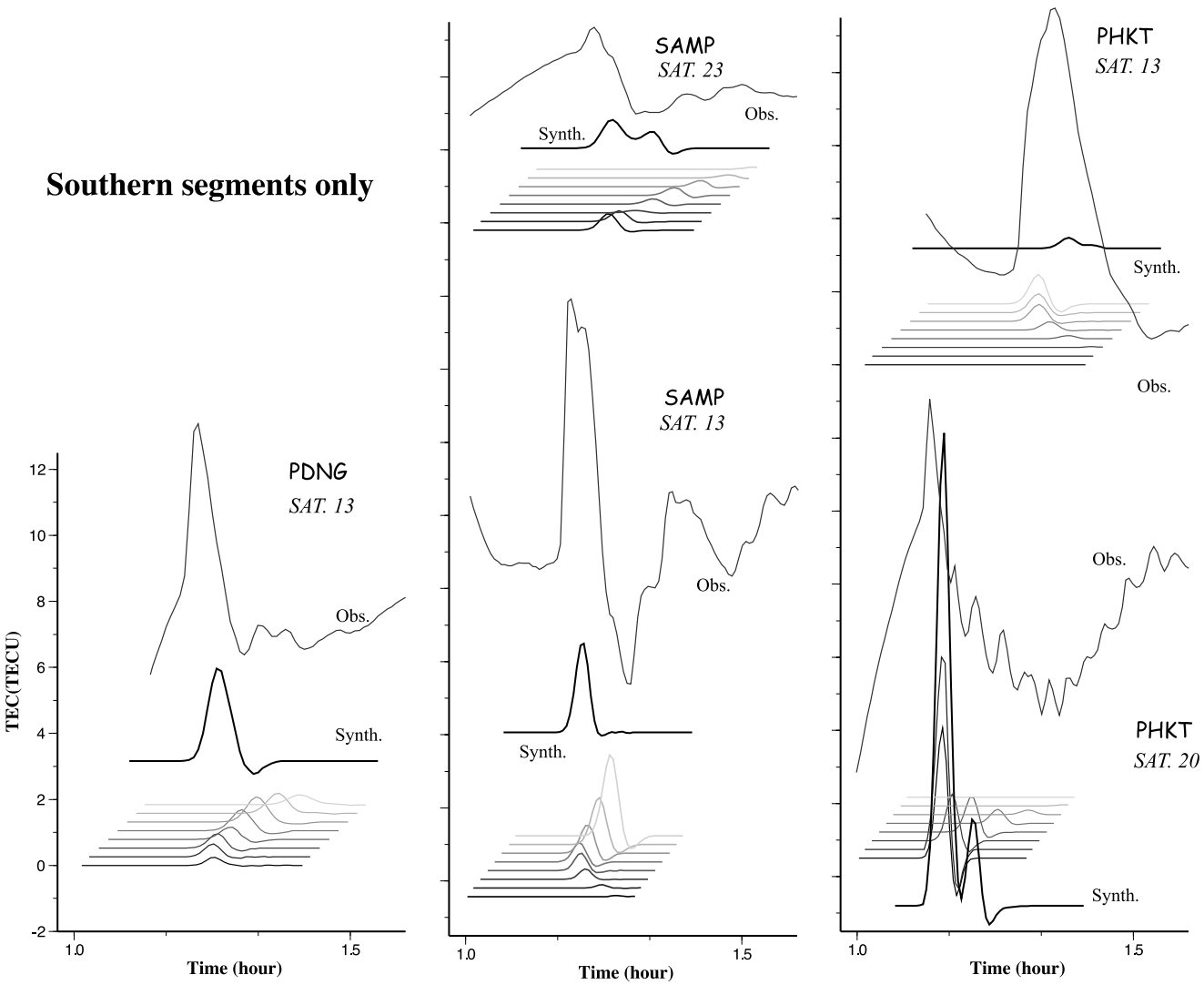

Figure 11. Same as Figure 9, but excitation from the northern half of the fault suppressed (Figure 6b).

waves. Our result thus supports the tsunami studies based on radar altimetry rather than conventional tide gauges.

4. Discussion and Conclusions

[27] We could further refine the fit in Figure 9, as mentioned earlier, by tuning the parameters in the original synthesis, e.g., relative magnitudes of individual sources and the rupture propagation speed. For example, the relatively poor semblance of PDNG-Sat.13 CID (a sharp peak seen in the observed CID is not well reproduced by synthesis) could be improved by making the sources 3 and 4 stronger. On the other hand, too large synthesized CID for PHKT-Sat.20 could be made smaller by reducing the weight of 1 and 2. Another way of improvement is by tuning the rupture propagation speed. By making the rupture propagation of the southern half faster, we can enhance the coherence of CIDs from southern sources and sharpen the PDNG-Sat.13 and SAMP-Sat.13 peaks.

[28] At the moment, we do not have firm external evidence to justify such ''improvement,'' and here just point out that such improvement is possible. As a different approach, we could substantially increase the number of point sources and perform an objective waveform inversion analysis by least squares fitting. Then, the obtained optimal solution for relative source amplitudes would be of some geophysical implication. Such a least squares approach, however, may not work well for the current data unless we could completely remove the non-CID signals such as diurnal TEC changes.

[29] CID investigation has just started, and still has problems to be solved. For example, the wavelengths of earthquake origin acoustic waves are several hundreds of kilometers, a spatial scale similar to the height-dependent wave velocity structures. It is pointed out that simple ray tracing there may introduce some kinds of systematic errors, such as dispersion (S. Watada, University of Tokyo, personal communication, 2005). Follow-on waves with smaller magnitudes are seen in SAMP-Sat.13 and PHKT-Sat.20, but their mechanism has not been modeled here yet. Influence of winds and atmospheric irregularities also need future investigations. Contribution from the subsided zone to the east of the uplifted zone is not evaluated here. It may have caused minor negative peaks preceding the main phase at SIPs east of the fault. However, they may be difficult to

detect because their time lags are only 1–2 min. Generally speaking, atmosphere is well mixed and CID seems to have virtue of simplicity in propagation theory when compared with those of seismic wave in the Earth's interior and tsunami in the ocean with complicated coastlines and non-flat ocean bathymetry.

[30] Seismological data from worldwide deployed seismometers are widely used to constrain earthquake source processes [e.g., *Ammon et al.*, 2005]. Broadband seismometers have sensitivity to periods longer than a few minutes, but relatively short-period components in surface waves are used to evaluate magnitudes of earthquakes and they often underestimate their sizes [*Stein and Okal*, 2005]. Tsunami data, in contrast, are useful to constrain faulting as slow as a few tens of minutes. CID provides another kind of useful information on faulting between seismic and tsunami bands. An advantage of CID over tsunami is that tide gauges can be installed only along coasts while GPS receivers can be put anywhere (even GPS receivers on buoys can measure CID owing to the geometry-free nature of the observable). One GPS station provides as many SIPs as the number of satellites received, and could provide multiple CID observations (Figure 3). In the present case, the CID appeared much earlier than the tsunami attacks in Thailand and Sri Lanka, and CID monitoring could serve as a part of early tsunami warning systems.

[31] We conclude the present study as follows: (1) Various waveforms and relative amplitudes of CIDs were observed after the 2004 great Sumatra-Andaman earthquake at nine GPS stations in Indonesia and Thailand. (2) Linearly distributed sources that excited sound wave sequentially from south to north can reproduce the observed CID signals to some extent. (3) The observed CIDs prefer rupture propagation speed of 2.5 to 1.7 km/s. (4) The northern half of the fault has excited CIDs as well as the southern half. (5) Rupture of the northern half was slow enough to be overlooked in seismograms but fast enough to excite atmospheric acoustic waves.

[32] **Acknowledgments.** We thank two anonymous referees and the Associate Editor for constructive reviews and Michio Hashizume, Chulalongkorn University, for GPS data in Thailand.

References

Ammon, C. J., et al. (2005), Rupture process of the 2004 Sumatra-Andaman earthquake, *Science*, *308*, 1133–1139.

Artru, J., T. Farges, and P. Lognonné (2004), Acoustic waves generated from seismic surface waves: Propagation properties determined from Doppler sounding observations and normal-mode modelling, *Geophys. J. Int.*, *158*, 1067–1077.

Artru, J., V. Ducic, H. Kanamori, P. Lognonné, and M. Murakami (2005), Ionospheric detection of gravity waves induced by tsunamis, *Geophys. J. Int.*, *160*, 840–848.

Banerjee, P., F. F. Pollitz, and R. Bürgmann (2005), The size and duration of the Sumatra-Andaman earthquake from far-field static offsets, *Science*, *308*, 1769–1772.

Calais, E., and J. B. Minster (1995), GPS detection of ionospheric perturbations following the January 17, 1994, Northridge earthquake, *Geophys. Res. Lett.*, *22*, 1045–1048.

Calais, E., J. B. Minster, M. A. Hofton, and M. A. H. Hedlin (1998), Ionospheric signature of surface mine blasts from global positioning system measurements, *Geophys. J. Int.*, *132*, 191–202.

DasGupta, A., A. Das, D. Hui, K. K. Bandyopadhyay, and M. R. Sivaraman (2006), Ionospheric perturbations observed by the GPS following the December 26th, 2004 Sumatra-Andaman earthquake, *Earth Planets Space*, *58*, 167–172.

Ducic, V., J. Artru, and P. Lognonné (2003), Ionospheirc remote sensing of the Denali earthquake Rayleigh surface wave, *Geophys. Res. Lett.*, *30*(18), 1951, doi:10.1029/2003GL017812.

Fujii, Y., and K. Satake (2005), Tsunami source model of the 2004 Sumatra-Andaman earthquake inferred from tide gauge and satellite data, *Eos Trans. AGU*, *86*(52), Fall Meet. Suppl., Abstract U11A-0807.

Galushko, V. G., V. V. Paznukhov, Y. M. Yampolski, and J. C. Foster (1998), Incoherent scatter radar observations of AGW/TID events generated by the moving solar terminator, *Ann. Geophys.*, *16*, 821–827.

Georges, T. M. (1968), H.F. Doppler studies of traveling ionospheric disturbances, *J. Atmos. Terr. Phys.*, *30*, 735–746.

Heki, K. (2006), Explosion energy of the 2004 eruption of the Asama Volcano, central Japan, inferred from ionospheric disturbances, *Geophys. Res. Lett.*, *33*, L14303, doi:10.1029/2006GL026249.

Heki, K., and J.-S. Ping (2005), Directivity and apparent velocity of the coseismic ionospheric disturbances observed with a dense GPS array, *Earth Planet. Sci. Lett.*, *236*, 845–855.

Hirata, K., K. Satake, Y. Tanioka, T. Kuragano, Y. Hasegawa, Y. Hayashi, and N. Hamada (2006), The 2004 Indian Ocean tsunami: Tsunami source model from satellite altimetry, *Earth Planets Space*, *58*, 195–201.

Hooke, W. H. (1970), The ionospheric response to internal gravity waves: 1. The F2 region response, *J. Geophys. Res.*, *75*, 5535–5544.

Iyemori, T., et al. (2005), Geomagnetic pulsation caused by the Sumatra earthquake on December 26, 2004, *Geophys. Res. Lett.*, *32*, L20807, doi:10.1029/2005GL024083.

Kanamori, H., J. Mori, and D. G. Harkrider (1994), Excitation of atmospheric oscillations by volcanic eruptions, *J. Geophys. Res.*, *99*, 21,947–21,961.

Lay, T., et al. (2005), The great Sumatra-Andaman earthquake of 26 December 2004, *Science*, *308*, 1127–1133.

Le Pichon, A., P. Henry, P. Mialle, J. Vergoz, N. Brachet, M. Garcés, D. Drob, and L. Ceranna (2005), Infrasound associated with 2004-2005 large Sumatra earthquakes and tsunami, *Geophys. Res. Lett.*, *32*, L19802, doi:10.1029/2005GL023893.

Liu, J. Y., Y. B. Tsai, S. W. Chen, C. P. Lee, Y. C. Chen, H. Y. Yen, W. Y. Chang, and C. Liu (2006), Giant ionospheric disturbances excited by the M9.3 Sumatra earthquake of 26 December 2004, *Geophys. Res. Lett.*, *33*, L02103, doi:10.1029/2005GL023963.

Neetu, S., I. Suresh, R. Shankar, D. Shankar, S. S. C. Shenoi, S. R. Shetye, D. Sundar, and B. Nagarajan (2005), Comment on "The Great Sumatra-Andaman earthquake of 26 December 2004," *Science*, *310*, 1431a.

Okada, Y. (1992), Internal deformation due to shear and tensile faults in a half-space, *Bull. Seismol. Soc. Am.*, *82*, 1018–1040.

Otsuka, Y., et al. (2006), GPS detection of total electron content variations over Indonesia and Thailand following the 26 December 2004 earthquake, *Earth Planets Space*, *58*, 159–165.

Saito, A., et al. (2002), Observations of traveling ionospheric disturbances and 3-m scale irregularities in the nighttime F-region ionosphere with the MU radar and a GPS network, *Earth Planets Space*, *54*, 31–44.

Stein, S., and E. A. Okal (2005), Speed and size of the Sumatra earthquake, *Nature*, *434*, 581–582.

Tahira, M. (1994), Acoustic resonance of the atmosphere at 3.7 mHz, *J. Atmos. Sci.*, *52*, 2670–2674.

Tanioka, Y., Yudhicara, T. Kusunose, S. Kathiroli, Y. Nishimura, S. Iwasaki, and K. Satake (2006), Rupture process of the 2004 great Sumatra-Andaman earthquake estimated from tsunami waveforms, *Earth Planets Space*, *58*, 203–209.

Yuen, P. C., P. F. Weaver, and R. K. Suzuki (1969), Continuous, traveling coupling between seismic waves and the ionosphere evident in May 1968 Japan earthquake data, *J. Geophys. Res.*, *74*, 2256–2264.

Zhang, D. H., and Z. Xiao (2005), Study of ionospheric response to the 4B flare on 28 October 2003 using International GPS Service network data, *J. Geophys. Res.*, *110*, A03307, doi:10.1029/2004JA010738.

N. Choosakul, Department of Geology, Faculty of Science, Chulalongkorn University, Phayathai Road, Bangkok 10330, Thailand. (cnwatthn@geo.sc.chula.ac.th)

K. Heki, Division of Earth and Planetary Sciences, Hokkaido University, N10 W8, Kita-ku, Sapporo 060-0810, Japan. (heki@mail.sci.hokudai.ac.jp)

N. Hemmakorn, Department of Telecommunications, Faculty of Engineering, King Mongkut's Institute of Technology, Ladkrabang, Bangkok, 10520 Thailand. (khnarong@kmitl.ac.th)

T. Komolmis, Department of Electrical Engineering, Faculty of Engineering, Chiang Mai University, Chiang Mai, 50200 Thailand. (tharadol@eng.cmu.ac.th)

T. Maruyama, National Institute of Information and Communications Technology, 4-2-1 Nukui-Kita, Koganei-city, 184-8795 Tokyo, Japan. (tmaru@nict.go.jp)

Y. Otsuka, Solar Terrestrial Environment Laboratory, Nagoya University, Honohara, Toyokawa-city, Aichi 442-8507, Japan. (otsuka@stelab.nagoya-u.ac.jp)